Schweizerischer Erdbebendienst
Service Sismologique Suisse
Servizio Sismico Svizzero
Swiss Seismological Service

ETH zürich

SITE CHARACTERIZATION REPORT

SVBE: Verbier École (VS), Switzerland

Agostiny Marrios Lontsi, Paolo Bergamo, Francesco Panzera, Donat Fäh

Last Modification: 20th August, 2022

Schweizerischer Erdbebendienst (SED)
Service Sismologique Suisse
Servizio Sismico Svizzero
Servizi da Terratrembels Svizzer

ETH Zürich
Sonneggstrasse 5
8092 Zürich
Schweiz
agostiny.lontsi@sed.ethz.ch

Contents

Summary

An active seismic survey was conducted at the strong-motion station SVBE at Verbier (VS) to characterize the underlying subsurface. Along the geophone' line, three broad-band velocitimeters were installed to record the ambient seismic vibrations. The seismic site characterization aims at using the recorded seismic signals to infer the shear-wave velocity profile around the installed seismological station.

The horizontal-to-vertical (H/V) spectral ratio analysis for the station SVBE62, that was built very close to the casing of SVBE, shows the main peaks at 4.11, 7.58, and 24.30 Hz with H/V amplitudes of 4, 6, and 8, respectively.

Two orthogonal lines of 24 geophones called L and T were set. The L-line had a two-meter geophone-spacing and the T-line had a half-meter geophone-spacing. The data from the L- and T-lines were analyzed using the multichannel analysis of surface waves method and the fundamental mode Rayleigh wave phase velocity dispersion curve was extracted between 18 and 48 Hz.

Two combined inversions are performed, where one invert the ellipticity and phase velocity dispersion curves, and the second invert the full H/V and the phase velocity dispersion curves. The first inversion indicates a velocity gradient in the first 20 meters and the second inversion indicate a shallow sediment cover with a gradient in the first 10 m.

The average V_{S30} from the two inversions are 371 $\pm$ 4 m/s and 437 $\pm$ 7 for the first and second inversion, respectively. This V_{S30} value corresponds to ground type B in EC8 (European standard) and C in SIA261 (Swiss standard).

1 Introduction

As part of the second phase of the Swiss Strong Motion Network renewal project, a strong motion station was built outside of a primary in Verbier. The station went operational on October 14^{th}, 2020. At this site, both an active and a passive seismic surveys were performed. We analyze the recorded active seismic data to extract the fundamental mode Rayleigh waves phase velocity dispersion curve. In a first inversion, the estimated fundamental mode ellipticity branches and the phase velocity dispersion information are combined to infer the underlying subsurface structure and the corresponding 1D shear wave velocity profile (e.g. Scherbaum et al. 2003; Hobiger et al. 2013). In a second inversion, the full H/V curve and the interpreted phase velocity dispersion information are combined (Lontsi et al., 2016).

2 Site and geological setting

Figure 1a) shows the location of Verbier in Switzerland. The zoom in Figure 1b) shows the surface geology around SVBE. It consists of glaciolacustrine sediments.

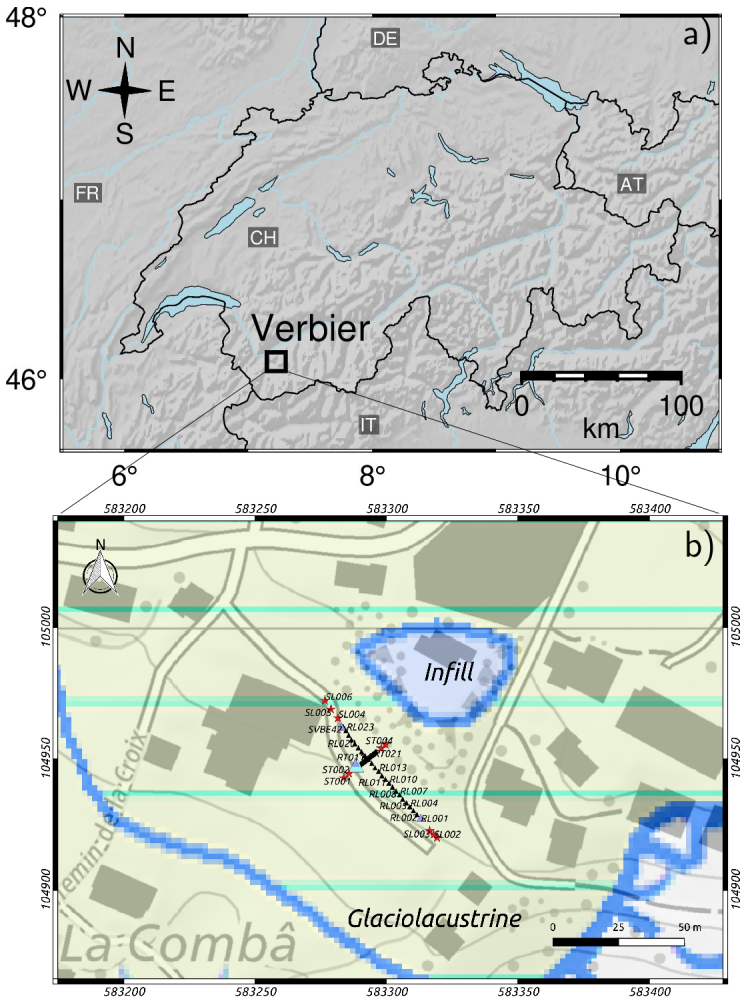

Figure 1: a) Location of the test site at Verbier (VS), Switzerland. b) A zoom of the test site where the strong motion station SVBE is located. The background image indicates the surface geology at the measurement site.

3 Overview of the active and passive seismic measurements

In order to characterize the local underground structure around station SVBE, an active and a passive seismic measurements were carried out on August 13^{th}, 2021.

3.1 Active seismic measurement

Figure 2 shows an aerial image of the survey site, indicating the location of the permanent station SVBE (turquoise triangle at the center). Two geophone lines were surveyed. The first line, called L, had a geophone spacing of $2m$. The second line, called T, had a geophone spacing of $0.5m$. Three sets of 8 4.5 Hz 3C geophones, resulting in 24 geophones, were used. The distinct geophone sets were connected with geode seismographs. One geode seismograph, south of the geophone line was connected to the field laptop, located in the car (Figure 3c).

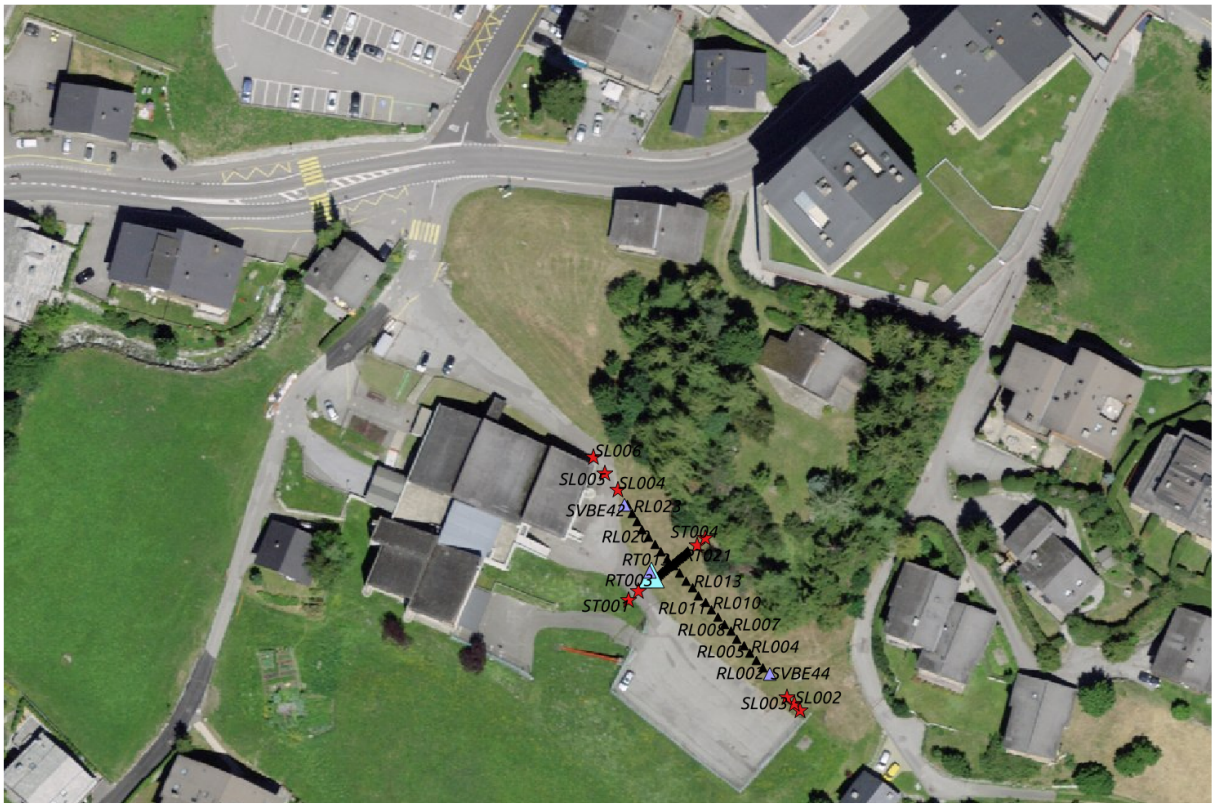

Figure 2: Background topography, strong motion station location (turquoise triangle), broadband sensors (purple triangle) and geophone lines (black triangle). ©2020 swisstopo (JD100042).

Two sledgehammers (metallic and non-metallic) were used to impact a metallic plate, that was placed on the ground, and to generate the seismic signal. The non-metallic sledgehammer is expected to generate seismic energy that is enriched at the lower frequencies (`http://www.masw.com/DataAcquisition.html`; Last accessed: 20^{th} August, 2022). Following Socco & Strobbia (2004) recommendations, different source-to-first-geophone offsets were used during the data acquisition. The source position was labeled with 5 letters. The first letter, S, stands for source, the second letter indicate the line that is being surveyed (L or T), the third letter indicates the sledgehammer being used

(metallic - H or non-metallic - G), the fourth letter is an integer number that indicates the source position number, and the blow's ID, such that the label SL001 indicates the source position 1 for the L geophone line and SLH12 indicates the second hammer blow for the source at the position 1, using a metallic hammer. For the L-line, the sledgehammer was used at 10 m (SL001), 8 m (SL002) , 6 m (SL003) to the most eastern geophone and at 4 m (SL004), 8 m (SL005) , 12 m (SL006) to the most western geophone of the line. For each source location, six hammer blows were performed, four blows used the metallic hammer and two blows used a non-metallic hammer.
For the T-line, the sledgehammer was used at 5.3 m (ST001), 2.7 m (ST002) to the most southern geophone and at 2.6 m (ST003), 4.9 m (ST004) to the most southern geophone. The same source label definition was used, such that STG21, for example, indicates the first hammer blow for the source at the position 2, using a non-metallic hammer. The source positions are marked with red stars on Figure 2. Figure 3 presents photographs from the field, and Figure 5 presents a screenshot of the active seismic database for Verbier. A sample hammer blow for the source ID SLH61 is presented in Figure 5.
The generated signal was recorded at $62.5\mu s$ sampling time interval and the signal was recorded for $1.5s$ with a delay of $-0.05s$.
Both the positions of the sources and geophones were measured by a differential GPS system (Leica Viva GS10) which was set up to measure with a precision better than 5 cm.

3.2 Passive seismic measurement

Along the L-line, three Lennartz 3C 5 s were positioned at the two ends, and at the center of the line to record ambient seismic vibrations. The recording at the distinct locations allows us to assess the variability of the subsurface along the surveyed line. The stations were labeled SVBE42, SVBE44, and SVBE42. The coupling of the censor to the ground was achieved through an aluminum tripod. The digitizer was a nanometric centaur and recorded the ambient seismic noise wavefield at a rate of 200 Hz. The station SVBE42 recorded the noise wavefield for 01 hour 19 min, from 09:15 to 10:34 UTC. The station was then dismantled to build the station SVBE62. SVBE62 recorded the noise wavefield for about 3 hours from 10:37 to 13:30 UTC. The station SVBE44 also operated continuously for about 3 hours, from 10:46 to 13:30 UTC. Some operational issued were encountered in the field. For example, the recorder of SVBE44 and SVBE42 showed a red LED status, that indicate a bad functioning of the stations. As a solution for station SVBE44, we changed one sensor cable and the battery that powers the digitiser. In the second case, we dismantled after about 1 hour of recording, the station SVBE42 to build the station SVB62. The original setting at this location was then dismantled.

Figure 3: Photographs from the field. Lines L and T geophone lines setup and the acquisition laptop. Paulina Janusz is the operator on the picture.

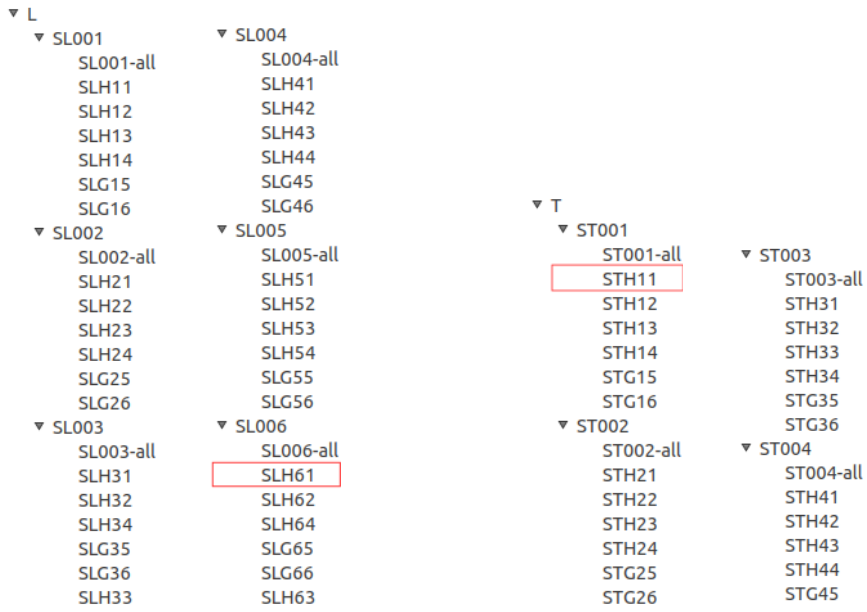

Figure 4: Screenshot of the active seismic database for Verbier. The red boxes around SLH01 and STH11 indicate the hammer blow that were used in the dispersion curves analysis.

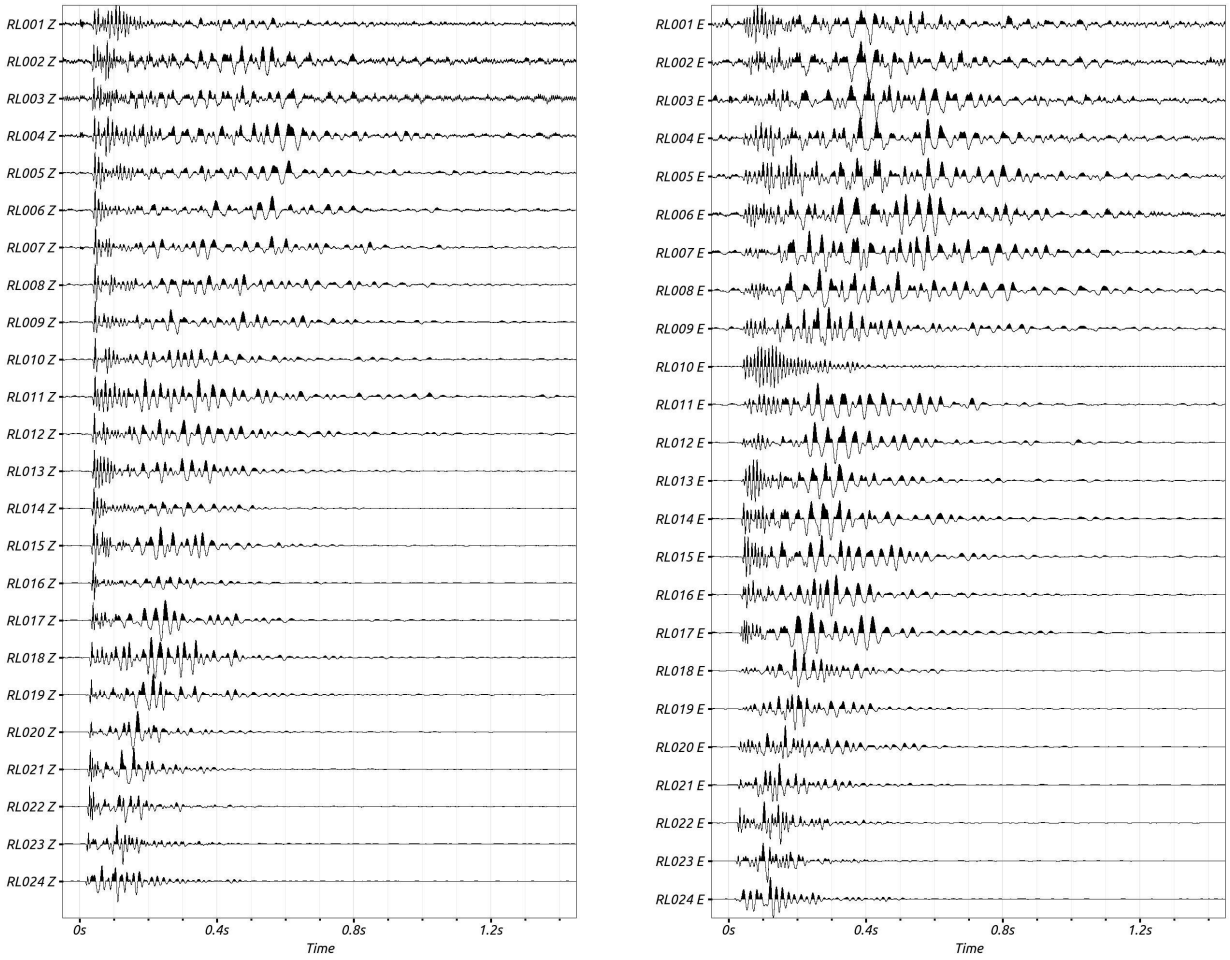

Figure 5: A sample hammer blow for the source ID SLH61. Left: vertical component. Right: Longitudinal component.

4 Single-station analysis of passive data

4.1 Microtremor H/V and ellipticity estimation

The microtremor H/V spectral ratio and the ellipticity curves are obtained using 6 different techniques:

- geopsyhv: full microtremor H/V estimation (www.geopsy.org);
- RayDec, optimized for Rayleigh wave ellipticity estimation (Hobiger et al., 2009);
- FTAN, optimized for Rayleigh wave ellipticity estimation (Fäh et al., 2009);
- CLASS, optimized for Rayleigh wave ellipticity estimation, (Fäh et al., 2001);
- VPTFA, optimized for Rayleigh wave ellipticity estimation (Poggi & Fäh, 2010);
- MTSPEC, optimized for Rayleigh wave ellipticity estimation (Burjánek et al., 2010).

The H/V results for each station using the 6 techniques are shown in Figure 6 for comparison. In general, the H/V spectral ratio shows a relatively stable peak at about 9 Hz. Given the topography of the site and the expected relatively shallow (few meters to few tens of meters) sediment cover, the peak frequency at about 1 Hz was overlooked, so that the difference in the frequency between the different curves is disregarded. The H/V curves along the L geophone line are presented in Figure 7. They show the variability of the curves along the line. The peak frequencies above 1 Hz are picked as shown in Figure 8.

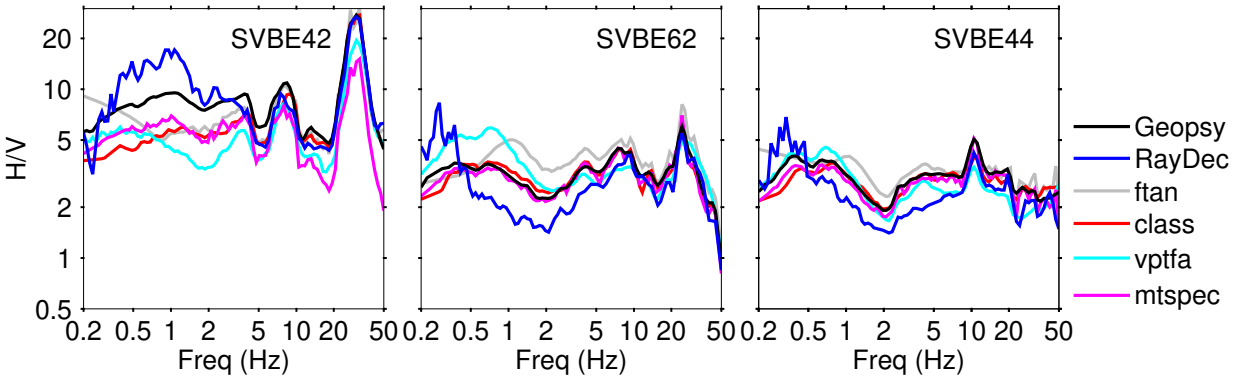

Figure 6: Obtained ellipticity and H/V spectral ratio curves using different techniques.

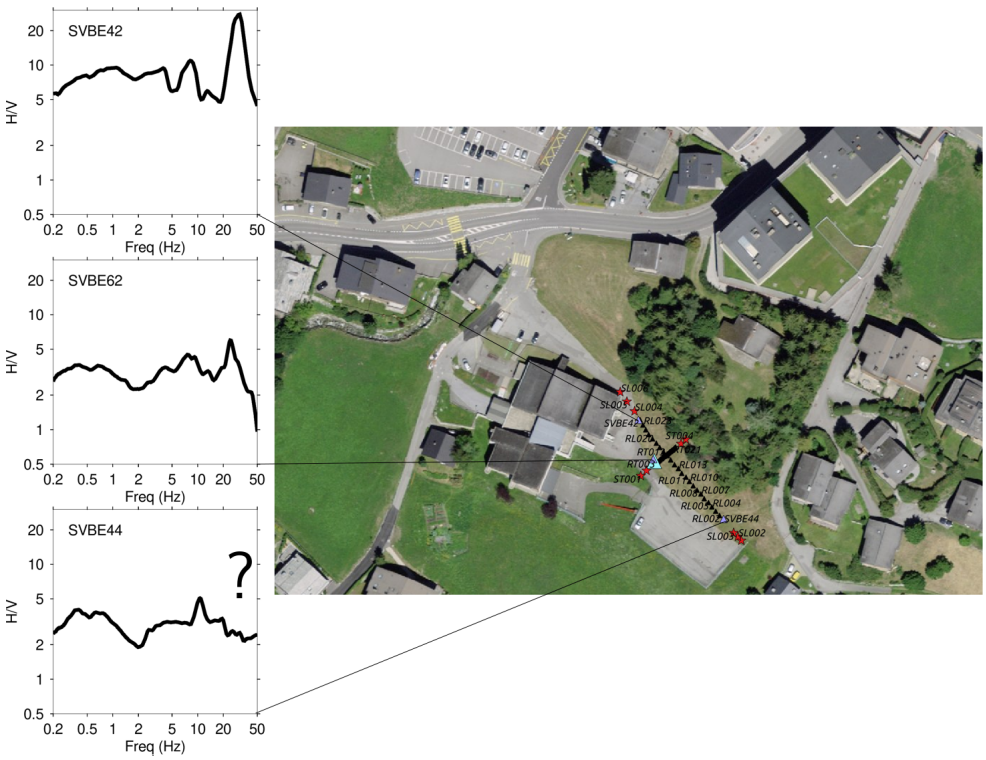

Figure 7: H/V variability along the L geophone line.

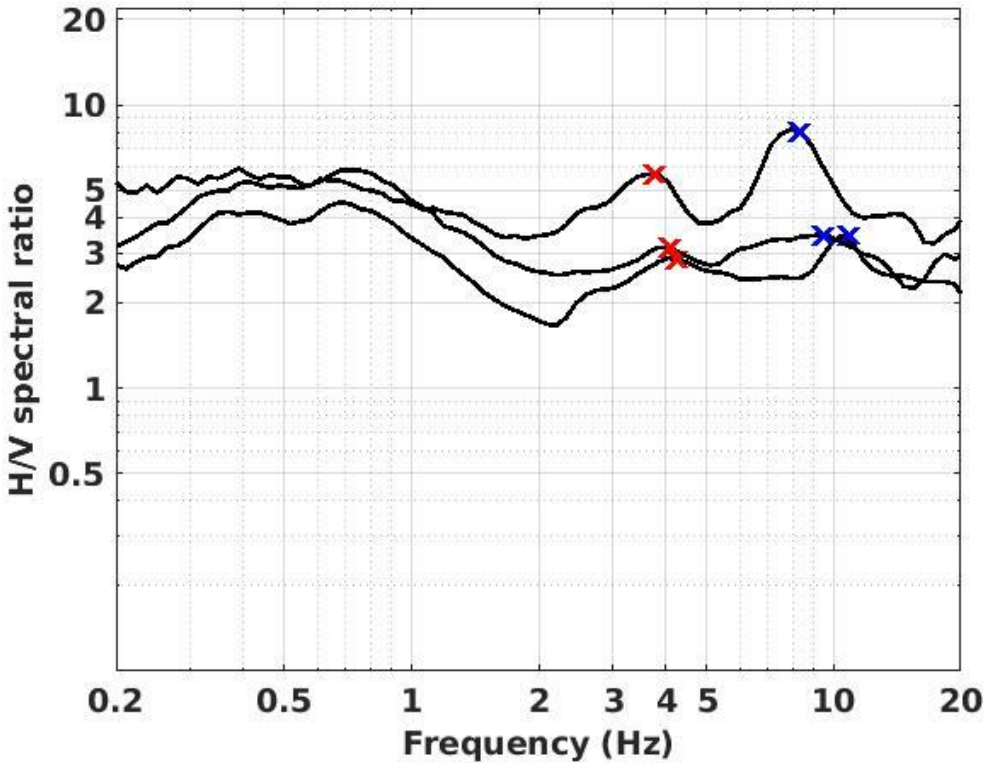

Figure 8: Overview of the H/V curves of the three stations, obtained using the ellipticity technique by Poggi & Fäh (2010); see also *vptfa* on Figure 6. The red and blue markers indicate the frequencies of the first and second maxima in the H/V spectral ratio curves.

4.2 Polarization analysis

Following Burjánek et al. (2010, 2012), the polarization analysis is performed to assess potential 2D effects. The results are shown in Figure 9 for station SVBE62, located very close to the permanent strong motion station SVBE. We observe no preferential strike direction and no indication for 2D polarization effects.

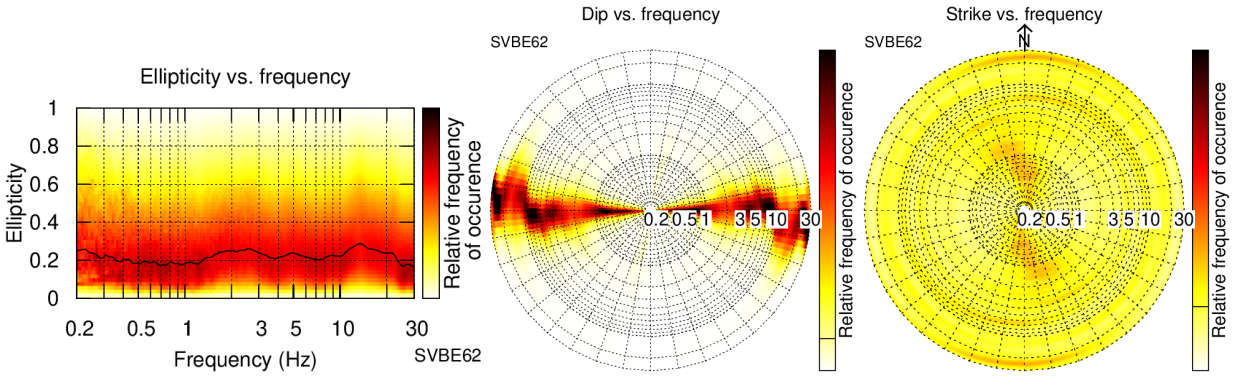

Figure 9: Polarization analysis for the station SVBE62 located next to the permanent station.

5 Array analysis of active seismic data

The phase velocity dispersion curves for Rayleigh waves is estimated for the L and T lines by using the frequency-wavenumber technique known as Multichannel Analysis of Surface Waves (MASW, Park et al. 1999) as implemented in geopsy. For the processing, we used the shot SLH61 and process the traces RL001 to RL021. The time window between 0 and 1.45 sec was used. We analyze the vertical and the longitudinal components. The beampower for the stack of recording was estimated for centered frequencies between 5 and 100 Hz on a logarithmic scale with a step of 0.1. Using a linear scale, 200 velocities were considered between 50 and 600 m/s. For the geophone line T, the time window between 0 and 0.5 sec was used.
The results of the dispersion curve analysis are presented in Figure 10. A phase velocity dispersion branch that is consistent with both the vertical and the longitudinal components is picked and overlaid on the other MASW results obtained using the data from STH11. Within the uncertainties, the estimated dispersion curves are in the same range for the L and T geophone lines.

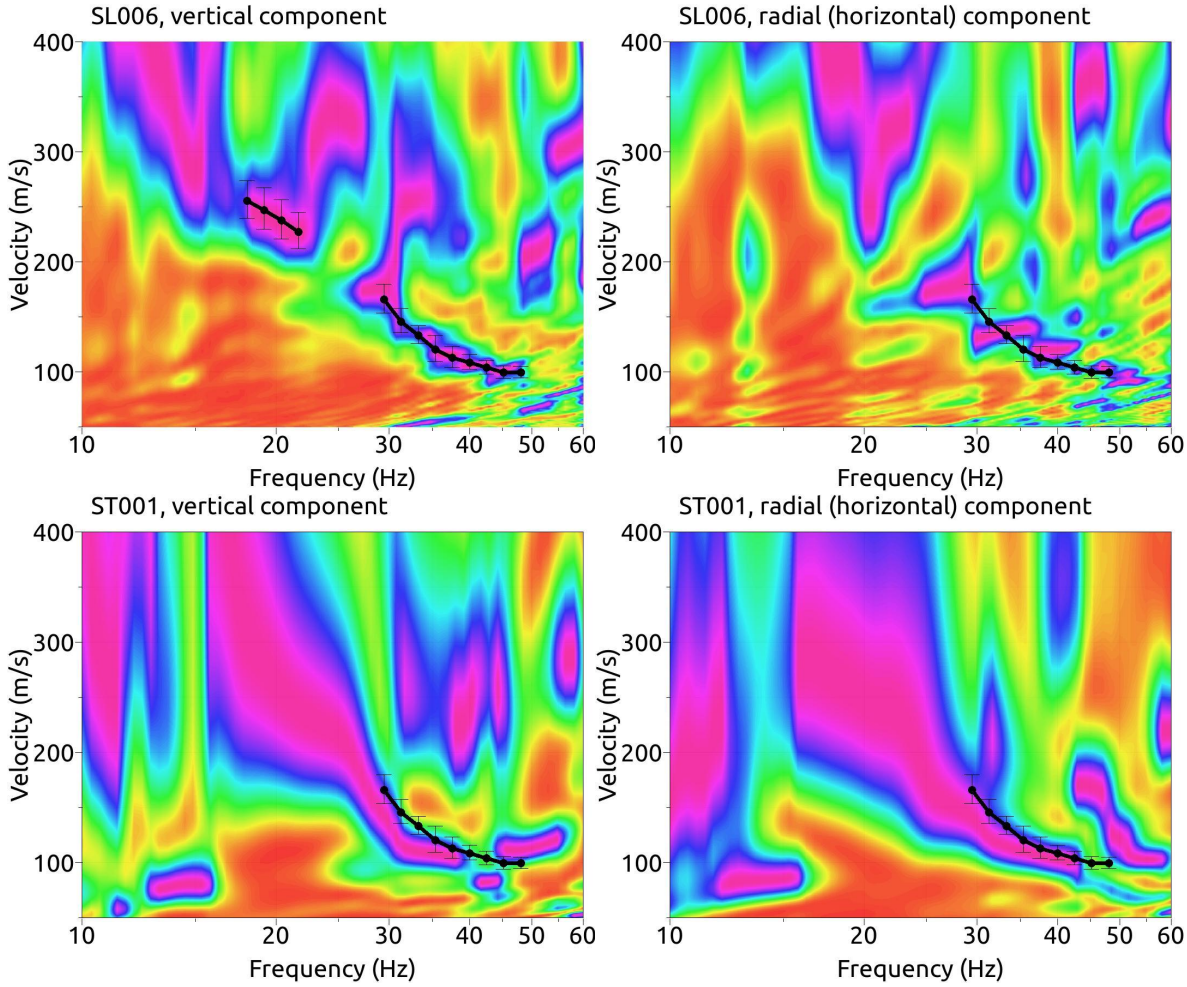

Figure 10: Top left: MASW results for SLH61, vertical component. Top right: MASW results for SLH61, longitudinal component. Bottom left: MASW results for STH11, vertical component. Bottom right: MASW results for STH11, longitudinal component. The dotted black line indicates the picked phase velocity dispersion curve from SLH61, vertical component. For comparison, the picked curve is overlaid on top of other MASW results.

6 Overview and discussion of the measurement results

Figure 11 presents an overview of the picked phase velocity dispersion curve, the ellipticity and the H/V curves. Assigning a mode number to the velocity dispersion branches is an important step towards a reliable combined inversion. Here, the two DC branches are interpreted as fundamental mode.
For the combined inversion, the ellipticity and dispersion curves are used in the first inversion. In a second inversion, full-hv-inv is used to invert the full spectrum of the microtremor H/V spectral ratio.

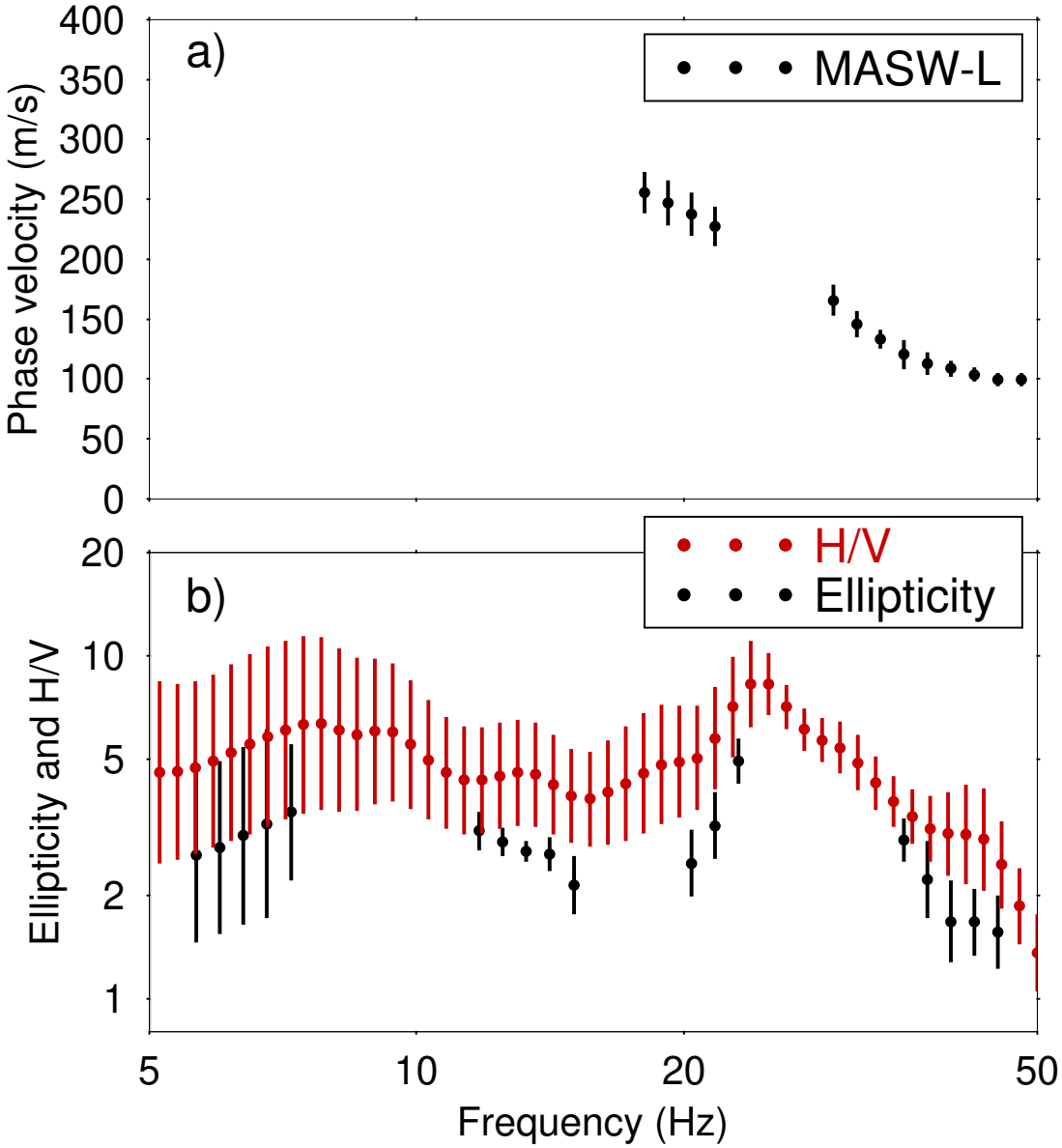

Figure 11: Overview of the results and interpreted curves obtained using the MASW and the single station methods. a) Phase velocity dispersion branches. b) Estimated microtremor H/V spectral ratio and Rayleigh wave ellipticity. Parts of the ellipticity curve, together with the peak frequency at 7.58 $\pm$ 0.76 Hz and the dispersion curves are used in the inversion. The microtremor H/V spectral ratio is used with full-hv-inv.

7 Joint inversion of dispersion and ellipticity curves

7.1 Parametrization

The inversion assumes a layered earth structure at the measurement site. Three, four, five, six and seven layers over half-space were used, as well as a parameter space with FixedLayer depths. The inversion uses the global search neighborhood algorithm (Sambridge, 1999; Wathelet, 2008). The process is started with a set of 50 models. In each iteration step, 50 new models are generated and the 50 best models are kept for further analysis. The process is iterated a large number of times to ensure that we sufficiently explore and exploit the parameter space.

7.2 Inversion results

Figures 21-17 show the Rayleigh wave (ellipticity and dispersion curves) inversion results. We summarize and interpret the best profiles from the inversion in Figure 26. Table 2 gives a summary of the minimum misfit values achieved in each case during the inversion process.

Table 1: Minimum misfit values for different parametrizations.

Parametrization	Minimum misfit
3 LOH	0.756
4 LOH	0.715
5 LOH	0.675
6 LOH	0.679
7 LOH	0.689
Fixedlayer	0.807

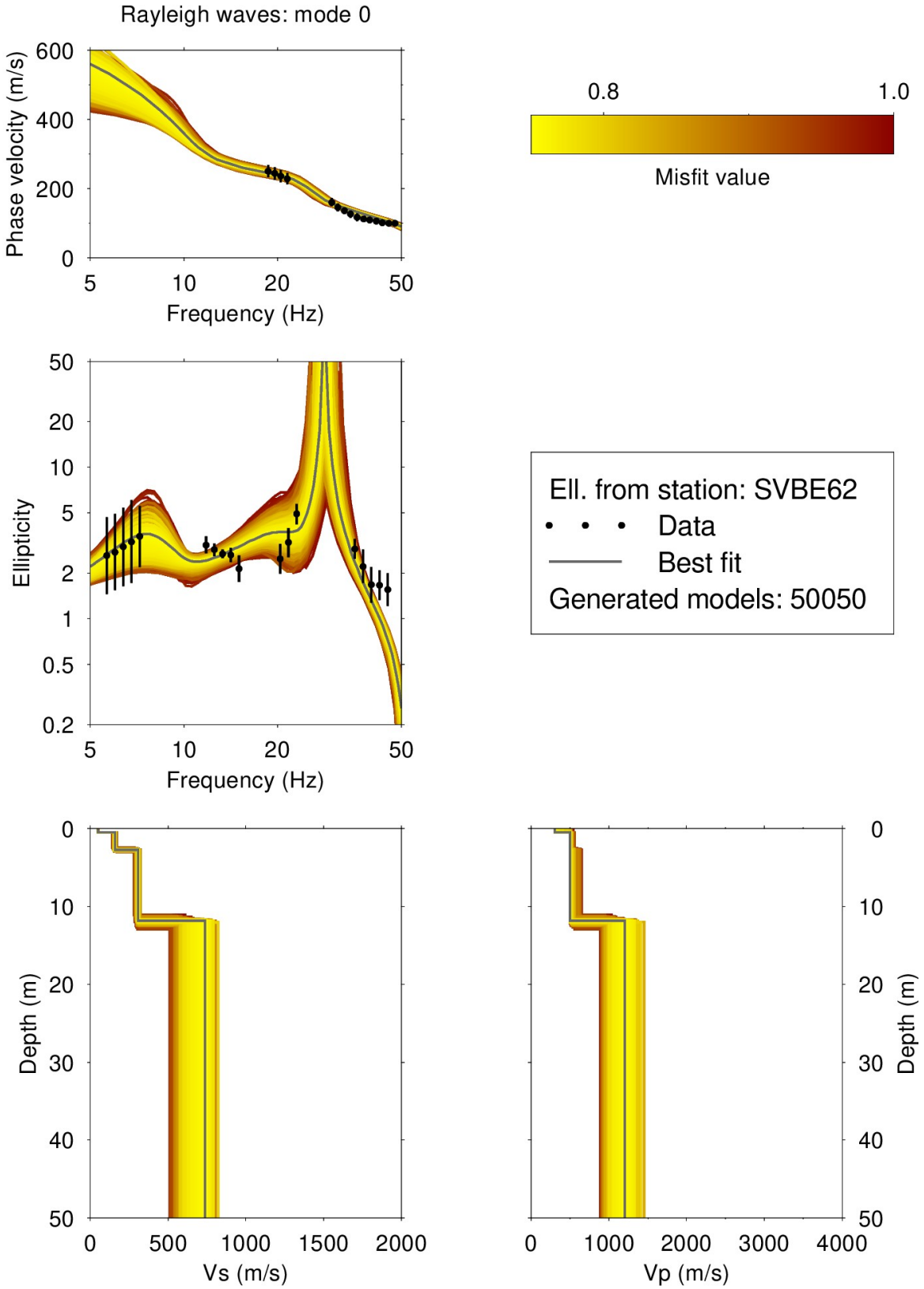

Figure 12: Inversion results using a 3LOH parametrization. The different models are shown in a color according to the misfit value, where the best model is shown in continuous grey color and the black dots indicate the data points that contribute to the inversion. The peak frequency at 7.58 ± 0.76 Hz is used as additional information to further constrain the bedrock depth.

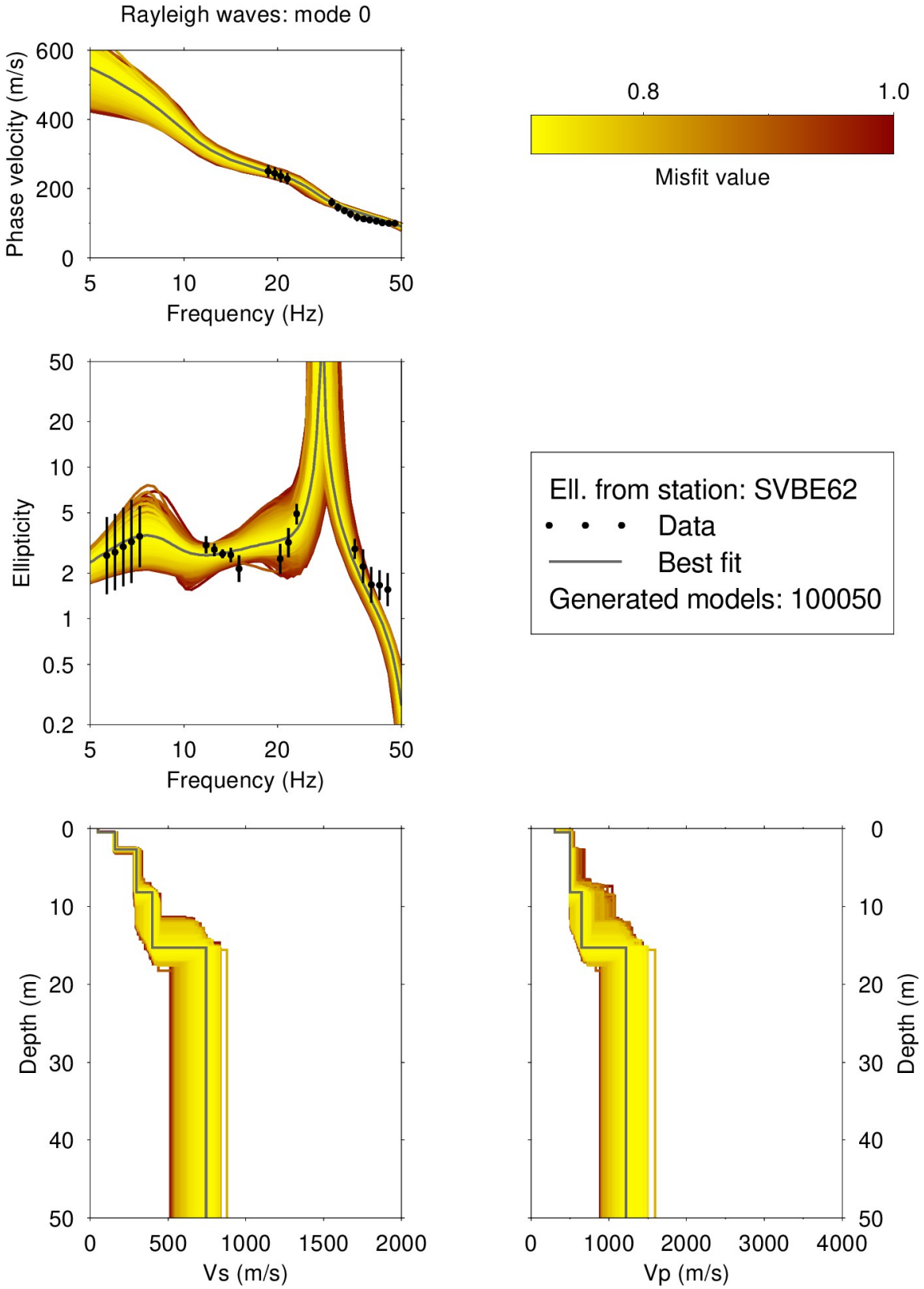

Figure 13: Inversion results using a 4LOH parametrization. The different models are shown in a color according to the misfit value, where the best model is shown in continuous grey color and the black dots indicate the data points that contribute to the inversion. The peak frequency at 7.58 ± 0.76 Hz is used as additional information to further constrain the bedrock depth.

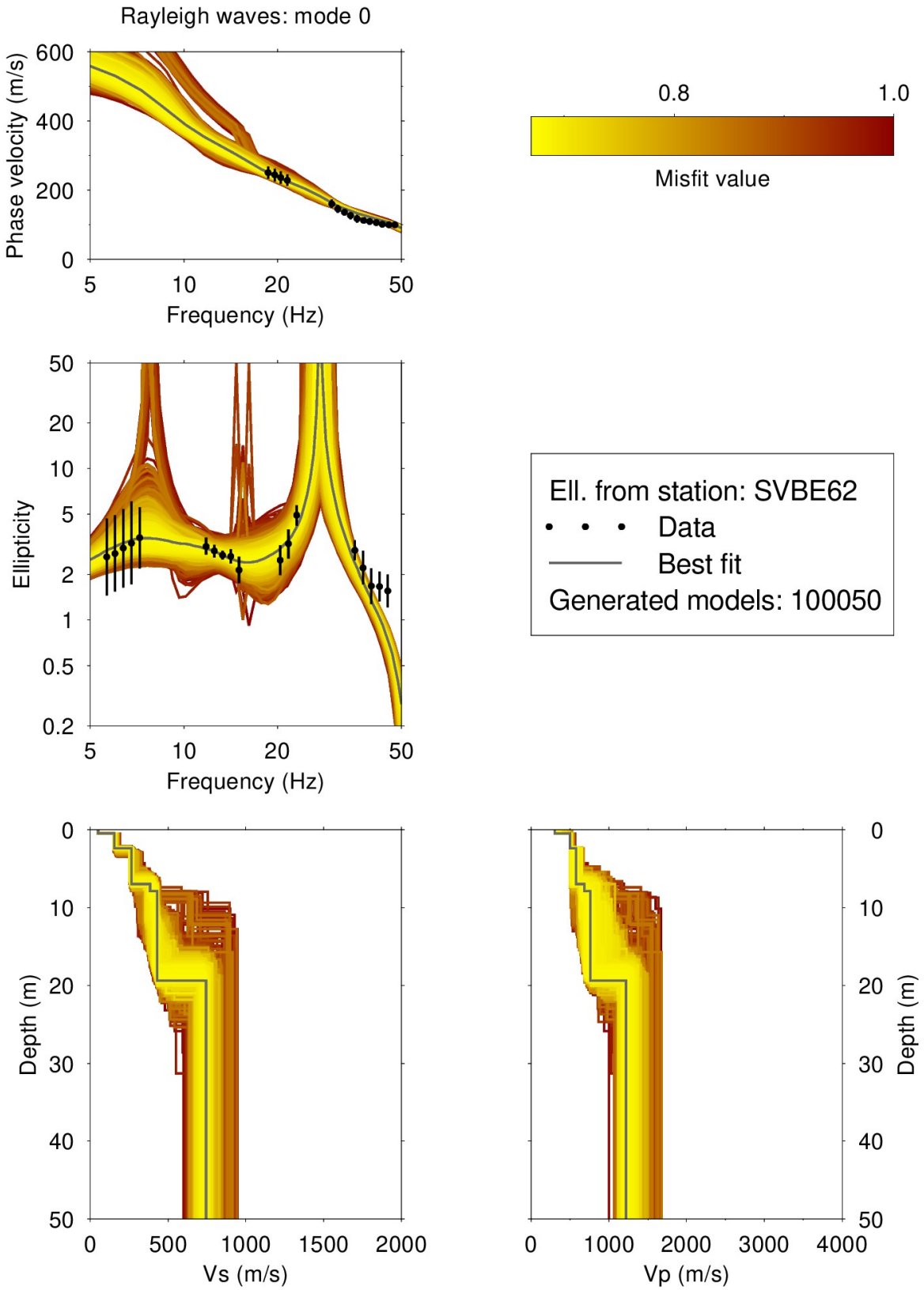

Figure 14: Inversion results using a 5LOH parametrization. The different models are shown in a color according to the misfit value, where the best model is shown in continuous grey color and the black dots indicate the data points that contribute to the inversion. The peak frequency at 7.58 ± 0.76 Hz is used as additional information to further constrain the bedrock depth.

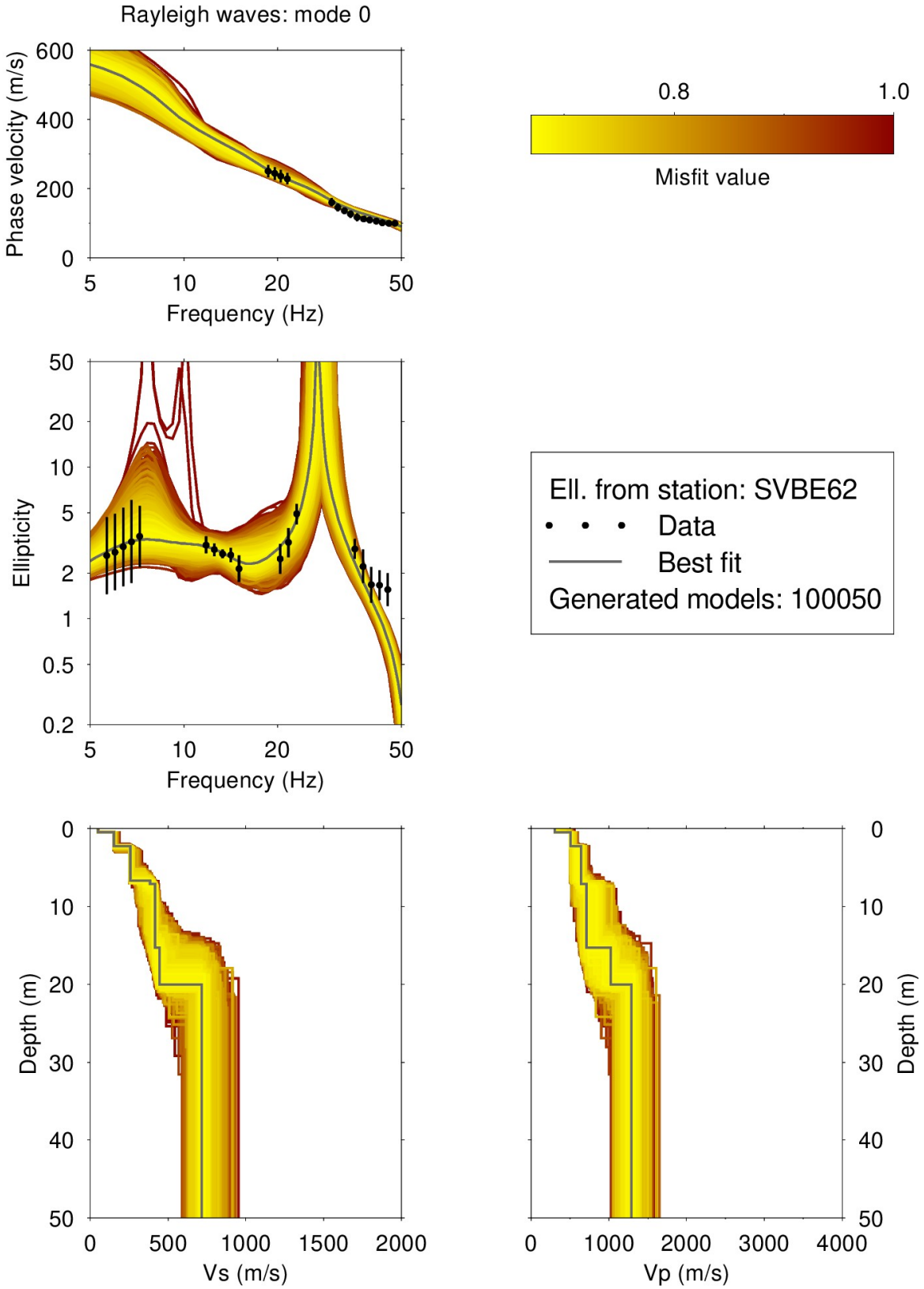

Figure 15: Inversion results using a 6LOH parametrization. The different models are shown in a color according to the misfit value, where the best model is shown in continuous grey color and the black dots indicate the data points that contribute to the inversion. The peak frequency at 7.58 ± 0.76 Hz is used as additional information to further constrain the bedrock depth.

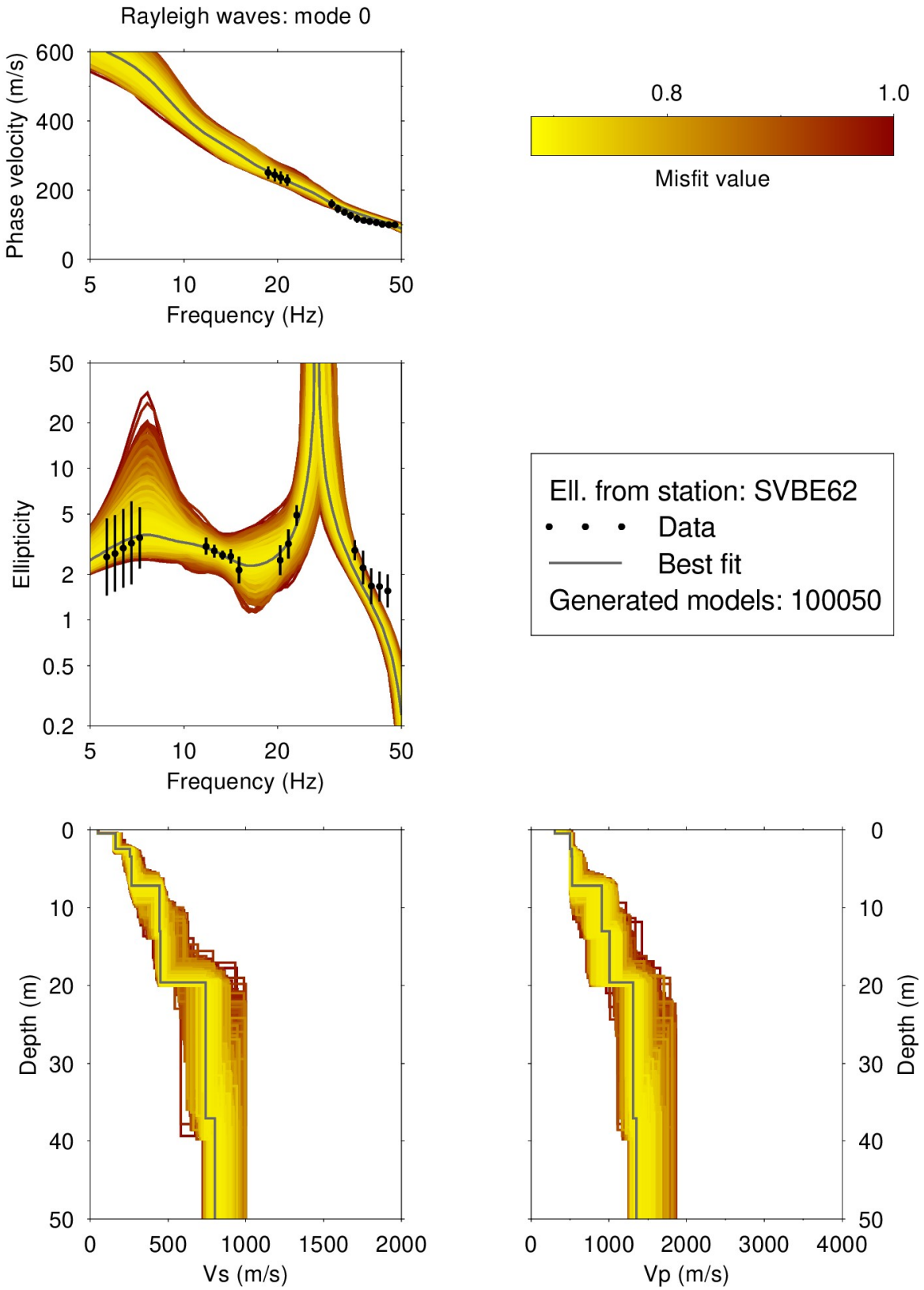

Figure 16: Inversion results using a 7LOH parametrization. The different models are shown in a color according to the misfit value, where the best model is shown in continuous grey color and the black dots indicate the data points that contribute to the inversion. The peak frequency at 7.58 ± 0.76 Hz is used as additional information to further constrain the bedrock depth.

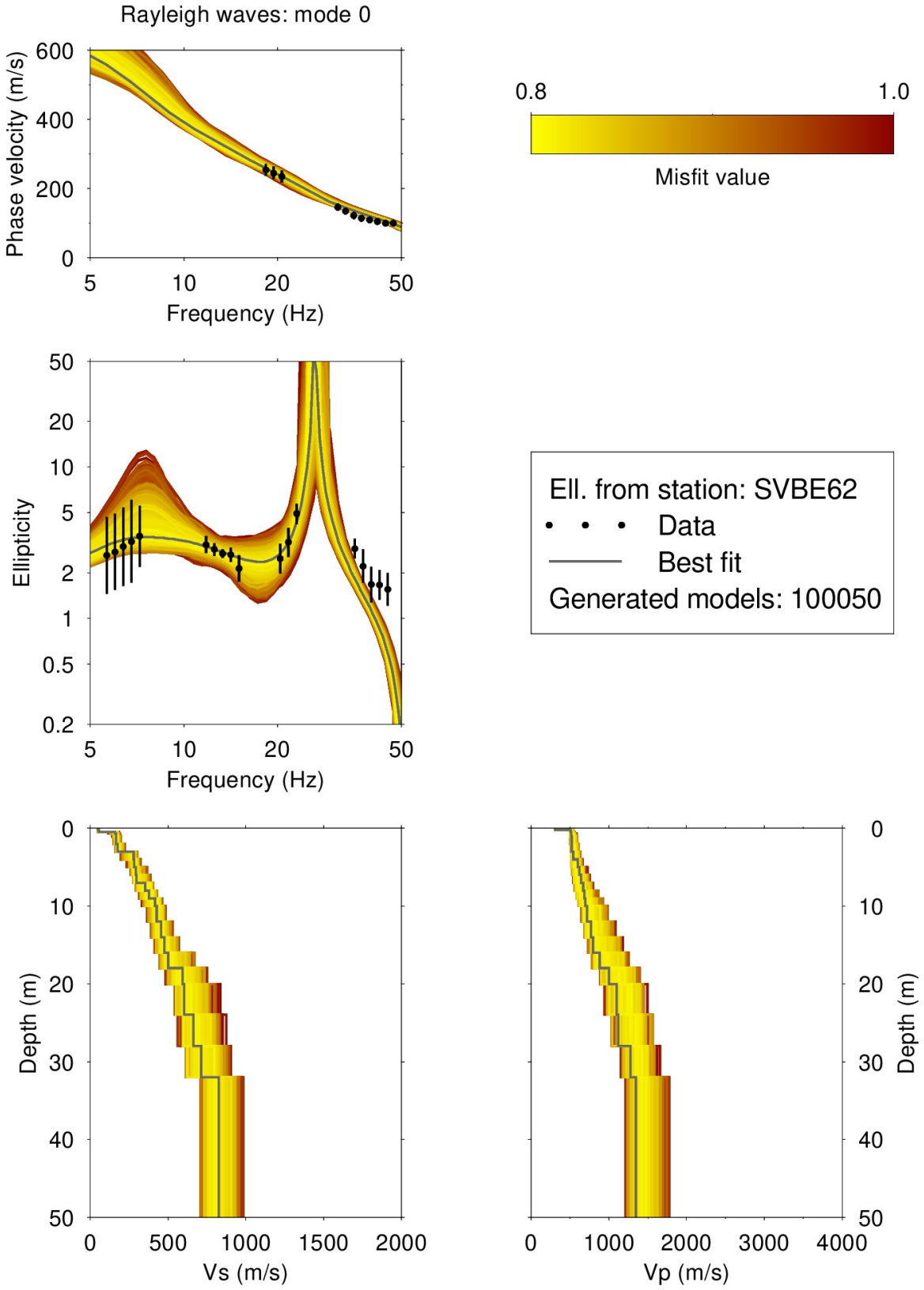

Figure 17: Inversion results using a FixedLayer thickness parametrization. The different models are shown in a color according to the misfit value, where the best model is shown in continuous grey color and the black dots indicate the data points that contribute to the inversion. The peak frequency at 7.58 $\pm$ 0.76 Hz is used as additional information to further constrain the bedrock depth.

7.3 Inversion summary

The best models from the inversions using different parametrizations (3LOH, 4LOH, 5LOH, 6LOH, 7LOH, and FixedLayer) are shown in Figure 26. The misfit values from the combined inversion vary between 0.6 and 0.9. A comparison of the S-wave velocity profiles indicate a velocity gradient in the first 10 m. The best velocity profiles from 3LOH and 4LOH parametrizations see discontinuity at 12 and 15 m depth, respectively. Other parametrizations indicate a discontnuity around 20 m. The average VS30 from this inversion is 371 $\pm$ 4 m/s. This VS30 value corresponds to ground type B in EC8 (European standard) and ground type C in SIA261 (Swiss standard).

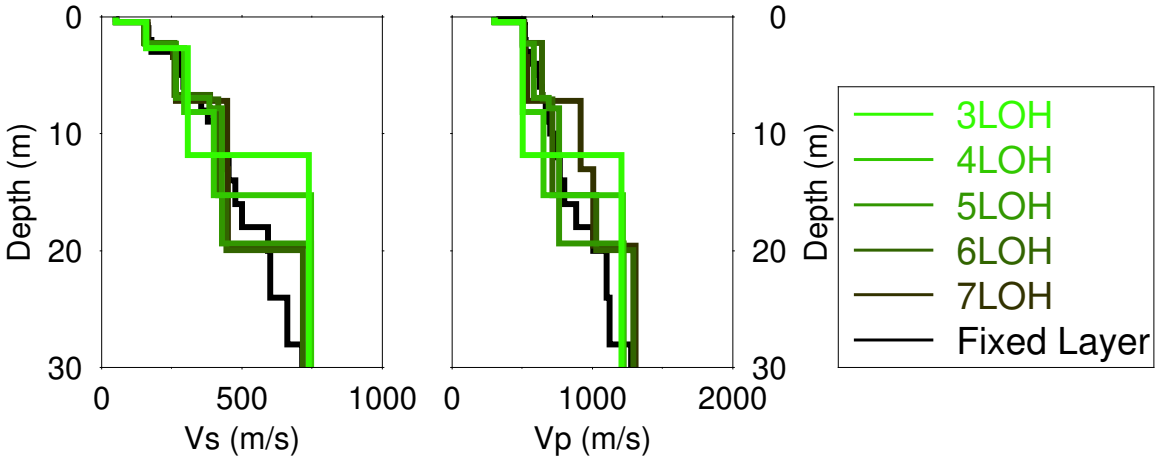

Figure 18: Overview of the best seismic velocity profiles for the different parameterizations.

7.4 Site amplification

Starting from the best models presented in Figure 26, the theoretical site amplification function is computed and compared with the empirical site amplification function of the station SVBE. For the calculation of the amplification, the seismic velocity profiles with 3LOH and 4LOH were excluded. The amplification referenced to the Swiss reference velocity profile is further used for comparison. The site amplification function is estimated following Edwards et al. (2013). The comparison is shown in Figure 19.

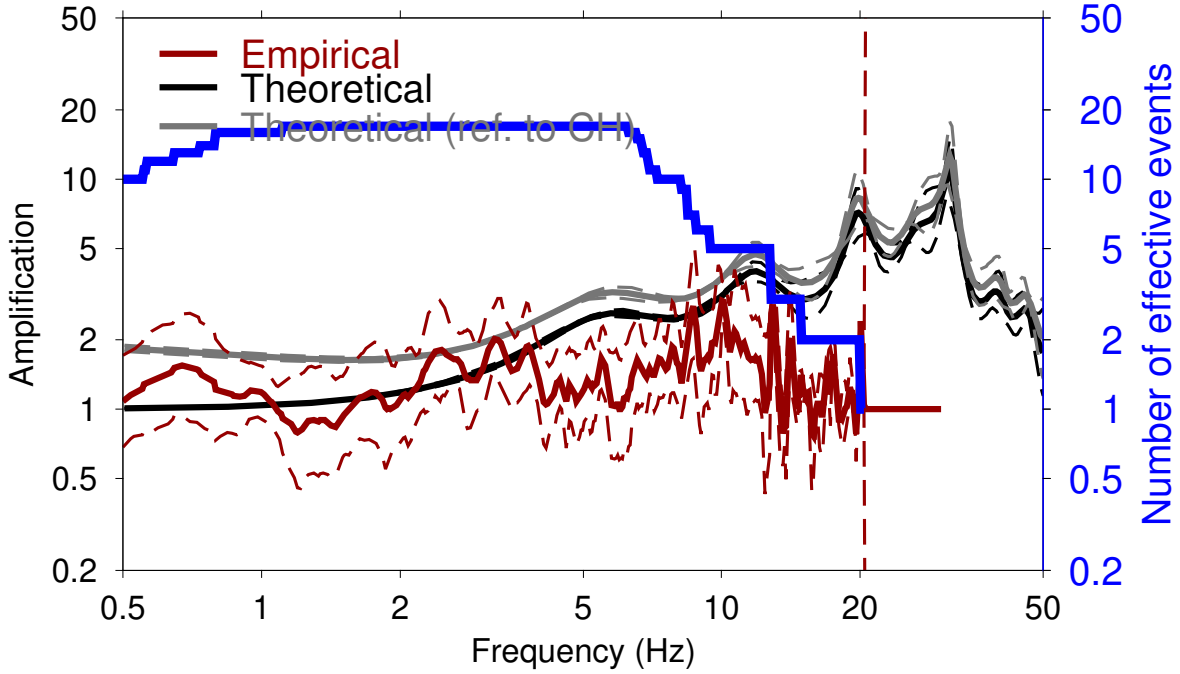

Figure 19: Comparison between the site amplification estimated with the best models from the inversions and the empirical amplification for station SVBE.

7.5 Quarter-wavelength representation

The quarter wavelength representation for the joint inversion of ellipticity and dispersion curves is presented in Figure 20.

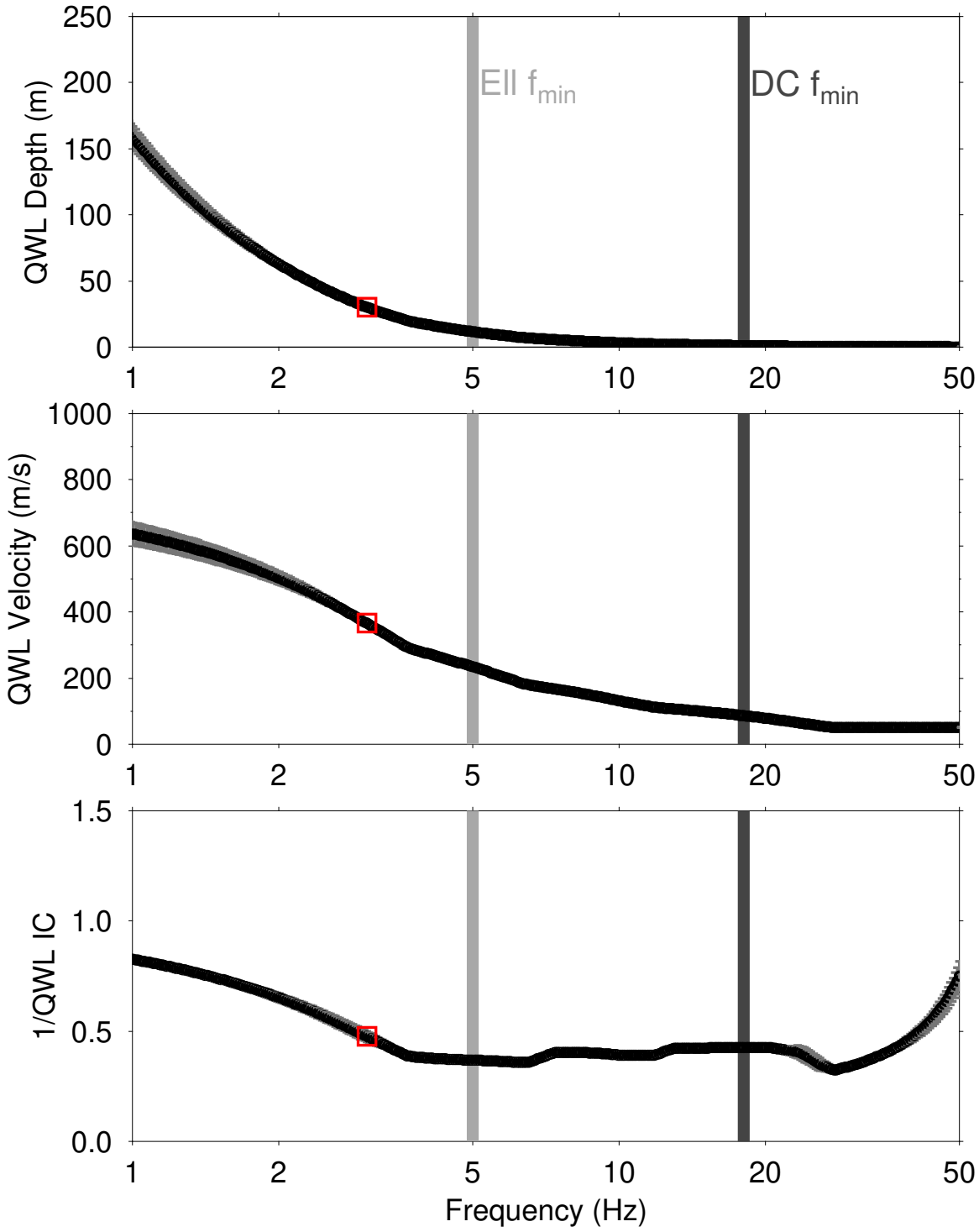

Figure 20: Quarter-wavelength representation for the best models of the inversions. The light and dark grey vertical bars indicate the minimum frequencies for the ellipticity and phase velocities, respectively, used in the inversion process. The solid black line uses all models from the inversion.

8 Joint inversion of full H/V and phase velocity dispersion curves

8.1 Parametrization

Similar to previous inversion, full-hv-inv assumes a layered earth structure. Three, four, five, six and seven layers over half-space were used. No parameter space with fixed depths was tested.

8.2 Results

Figures 21-17 show full-hv-inv results. We summarize and interpret the best profiles from the inversion in Figure 26. Table 2 gives a summary of the minimum misfit values achieved in each case during the inversion process.

Table 2: Minimum misfit values for different parametrizations.

Parametrization	Minimum misfit
3 LOH	0.572
4 LOH	0.435
5 LOH	0.373
6 LOH	0.387
7 LOH	0.385

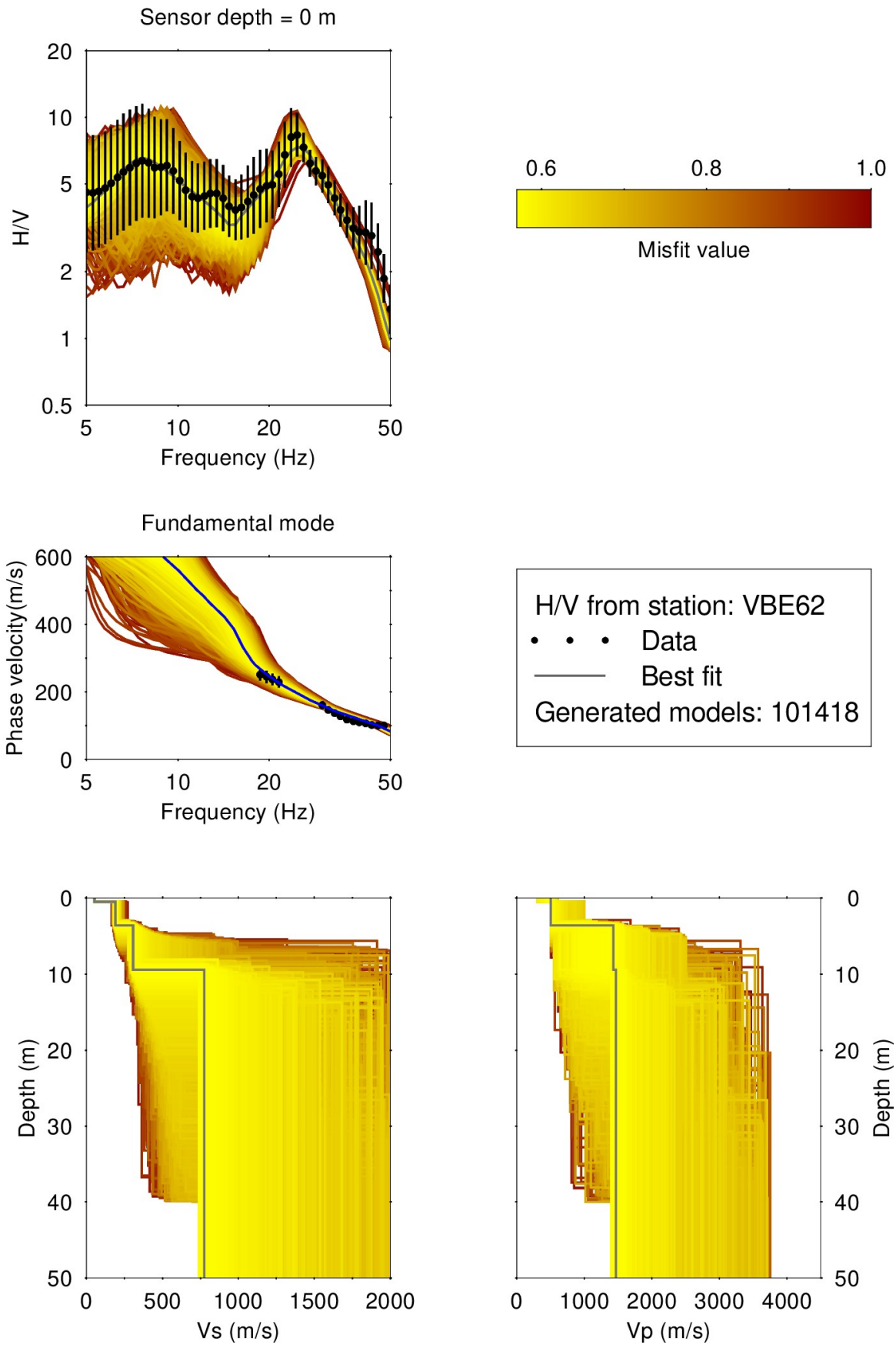

Figure 21: Full-hv-inv results using a 3LOH parametrization. The different models are shown in a color according to the misfit value, where the best model is shown in continuous blue color and the black dots indicate the data points that contribute to the inversion.

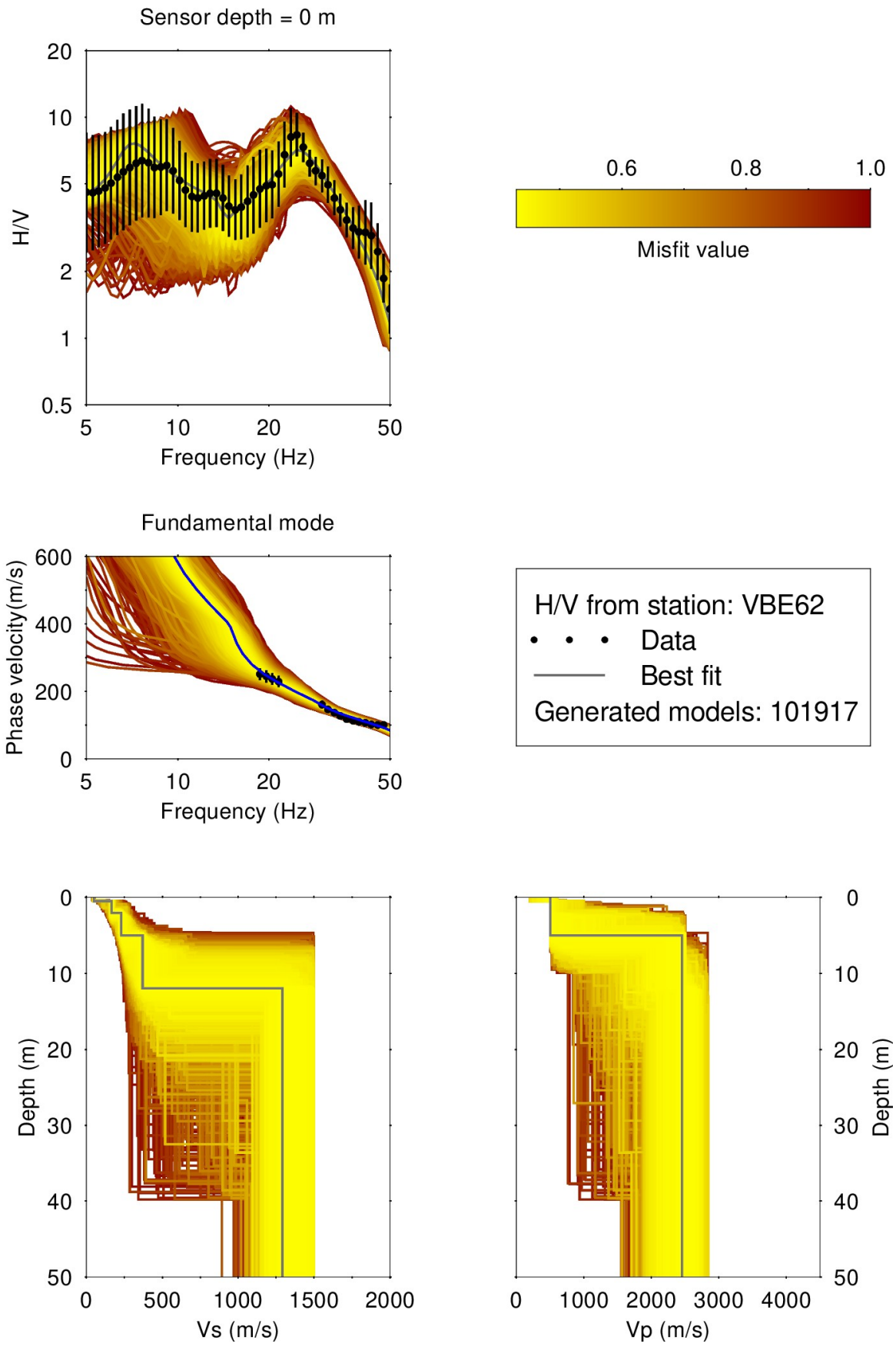

Figure 22: Full-hv-inv results using a 4LOH parametrization. The different models are shown in a color according to the misfit value, where the best model is shown in continuous blue line and the black dots indicate the data points that contribute to the inversion.

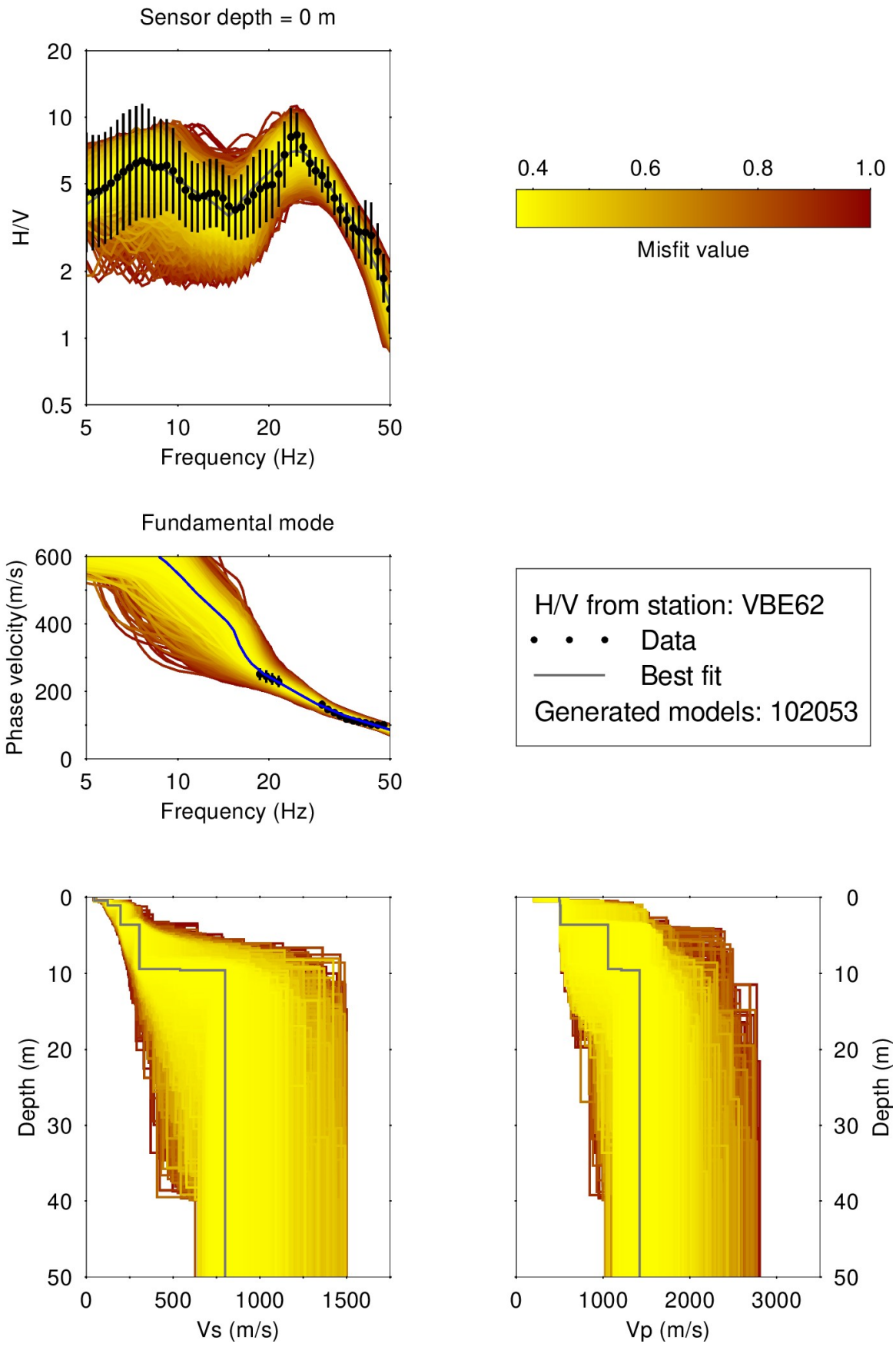

Figure 23: Full-hv-inv results using a 5LOH parametrization. The different models are shown in a color according to the misfit value, where the best model is shown in continuous blue line and the black dots indicate the data points that contribute to the inversion.

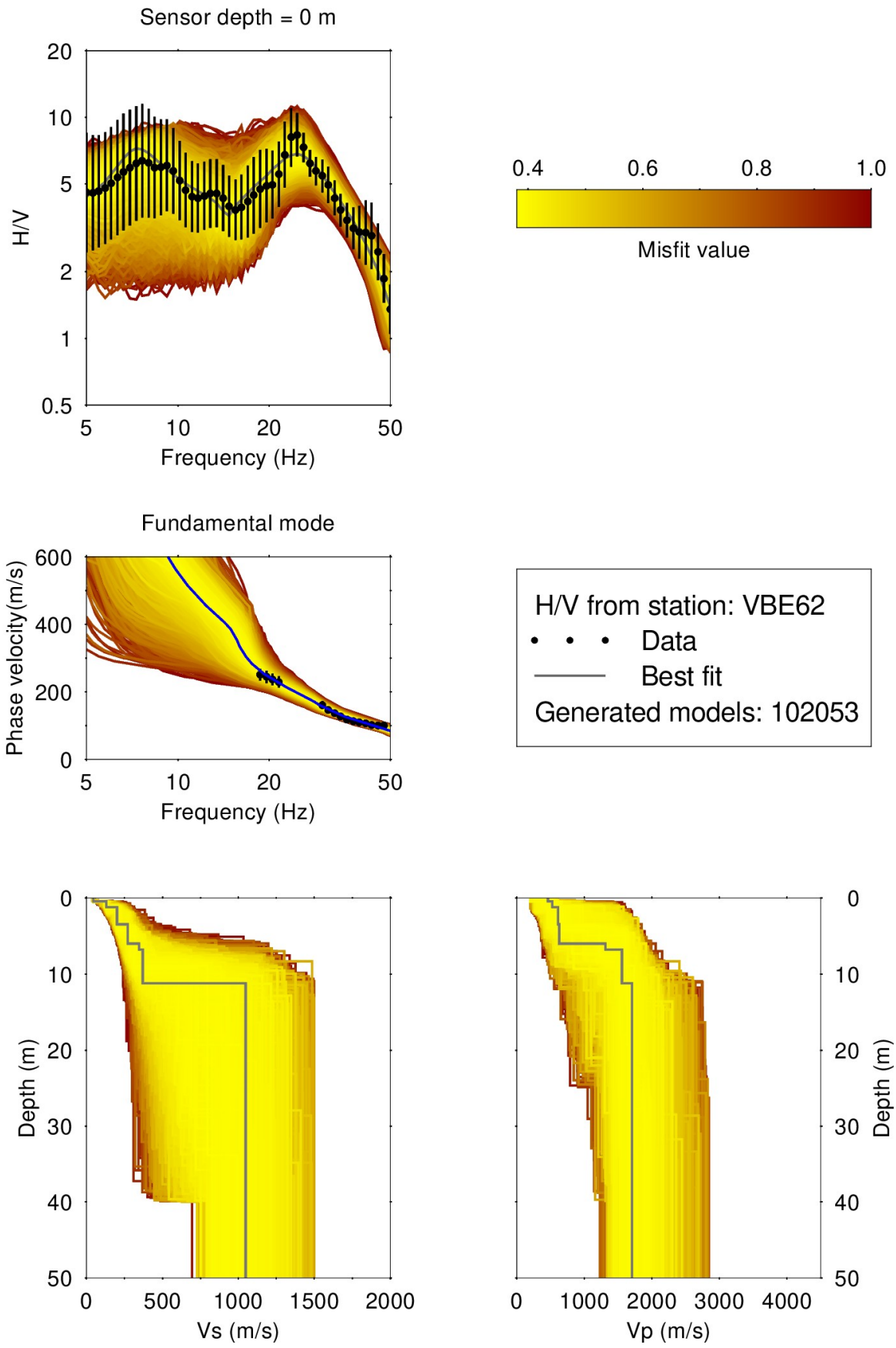

Figure 24: Full-hv-inv results using a 6LOH parametrization. The different models are shown in a color according to the misfit value, where the best model is shown in continuous blue line and the black dots indicate the data points that contribute to the inversion.

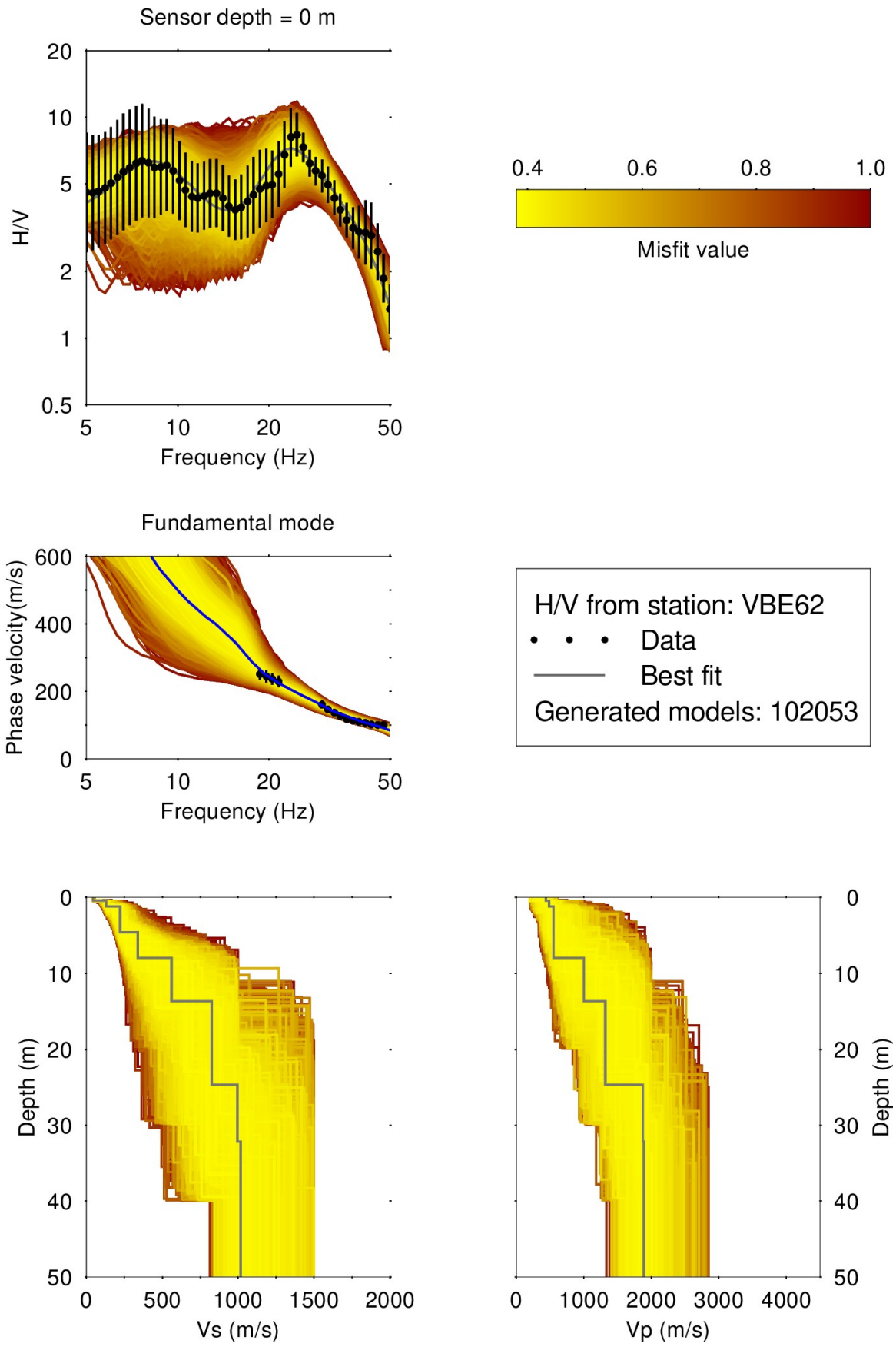

Figure 25: Full-hv-inv results using a 7LOH parametrization. The different models are shown in a color according to the misfit value, where the best model is shown in continuous blue line and the black dots indicate the data points that contribute to the inversion.

8.3 Inversion summary

The best models from the inversions using different parametrizations (3LOH, 4LOH, 5LOH, 6LOH, and 7LOH) are shown in Figure 26. The minimum misfit values from the combined inversion vary between 0.37 and 0.58. The average VS30 value is 437 $\pm$ 7 m/s. This VS30 value corresponds to the ground type B in EC8 (European standard) and C in SIA261 (Swiss standard).

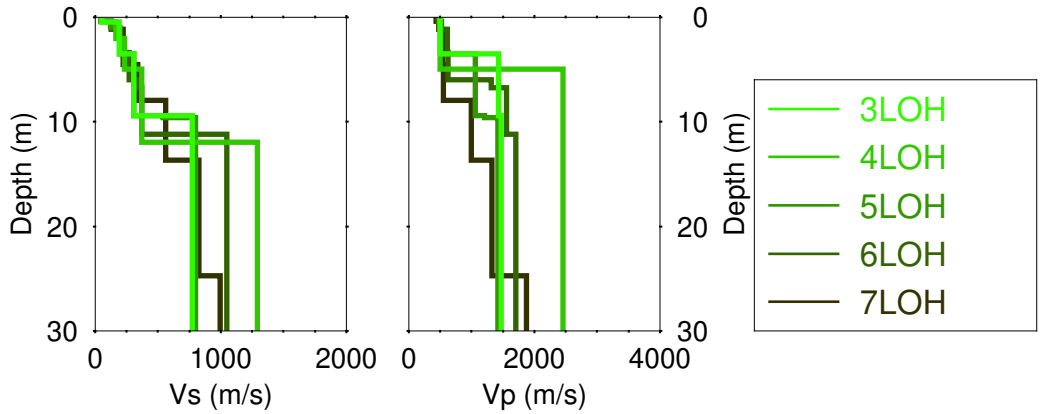

Figure 26: Overview of the best seismic velocity profiles for the different parameterizations.

8.4 Site amplification

Starting from the best models presented in Figure 26, the theoretical site amplification function is computed and compared with the empirical site amplification function of the station SVBE. The amplification referenced to the Swiss reference velocity profile is also used for comparison. The site amplification function is estimated following Edwards et al. (2013). The comparison is shown in Figure 19.

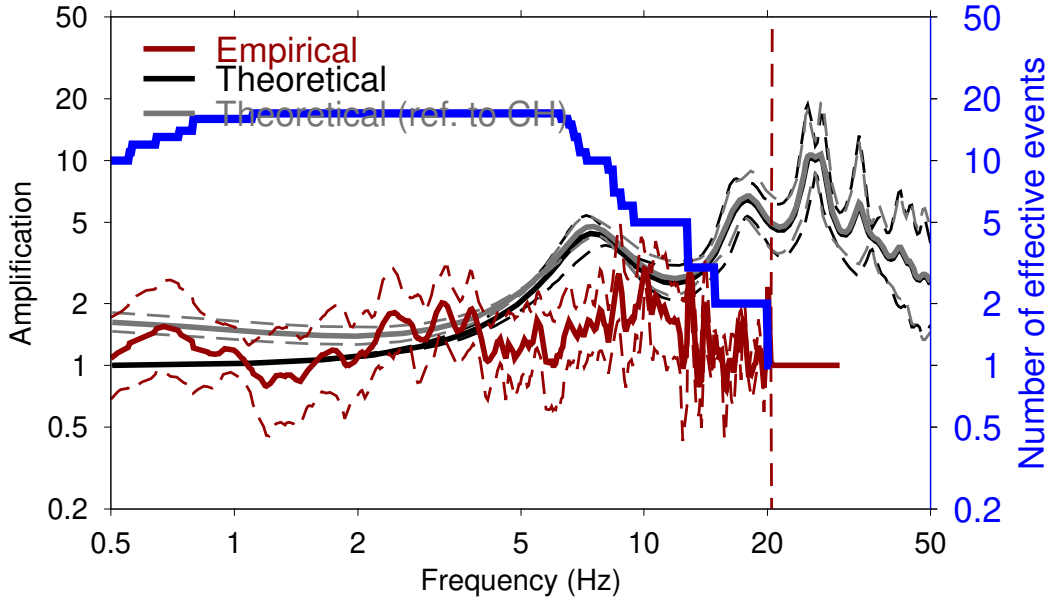

Figure 27: Comparison between the site amplification estimated for the best models from the inversions and the empirical amplification for station SVBE.

8.5 Quarter-wavelength representation

The quarter wavelength representation for this inversion is presented in Figure 28.

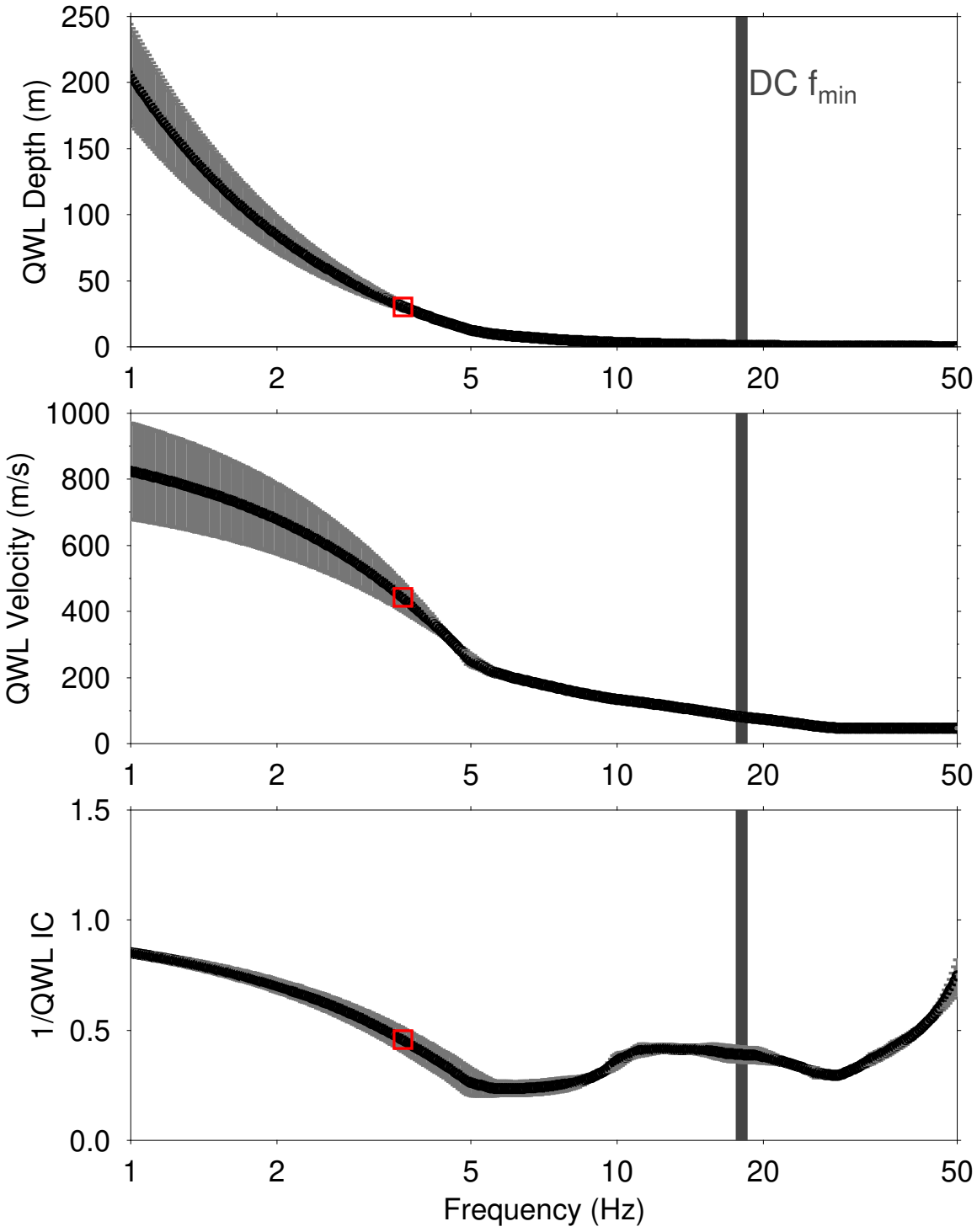

Figure 28: Quarter-wavelength representation for the best models of the inversions. The black vertical bars indicates the minimum frequency for the phase velocity that was used in the inversion process.

9 Summary of the two inversions

Table 3 presents a summary of the analysis and interpretation.

Table 3: Comparison of the site parameters from the two inversions.

Engineering parameters and site classification	Ell. + DC inversion	full-hv-inv
V_{S30}	371 ± 4 m/s	437 ± 7 m/s
f_0	7.58 Hz	
z_{800} Depth to engineering bedrock (Depth to shallowest layer exceeding $V_S = 800m/s$)	N/A	N/A
Soil class according to EC8	B	B
Soil class according to SIA	C	C

10 Conclusion

An active seismic measurement was carried out at the strong motion station SVBE at Verbier (VS) to characterize the local subsurface. The measurement was complemented by single station ambient vibration measurements along the geophone profile. In the frequency band between 18 Hz and 48 Hz, two phase velocity dispersion curves for Rayleigh waves were picked and assigned the fundamental mode. Two frequency peaks were measured for the H/V spectral ratio and ellipticity at around 7.58 and 24.30 Hz, where the peak at 24.30 Hz is dominant for SVBE. Two inversion were used: the first inversion used dinver to invert the ellipticity and dispersion curves as targets and the second inversion used full-hv-inv to invert the H/V spectral ratio and the dispersion curves. The left and right flanks of the ellipticity curves around the peak frequencies were used in the inversion. The results from dinver (ellipticity and peak frequency and dispersion curves) indicate a seismic velocity gradient in the first 10 m, a bedrock at around 20 m and a VS30 value of 371 ± 4 m/s. Full-hv-inv (H/V and dispersion curves) results indicate a seismic velocity gradient in the first 10 m and a VS30 value of 437 ± 7 m/s. The borehole log information available around the investigated site indicates a strong variability in the bedrock depth. The closest borehole gives a bedrock at 5 m. For the obtained VS30 values, the ground is classified as ground type B in EC8 (European standard) and C in SIA261 (Swiss standard). From the best velocity profiles obtained from the two inversions, the 1D SH-wave amplification were calculated in each case and the results were compared with the empirical spectral modeling curves obtained using earthquake data. The amplification functions from the two approaches are in the same amplitude range within the analyzed frequency band. However, the shape slightly differ around 10 Hz.

11 Acknowledgments

We thank Paulina Janusz for her assistance during field measurements.

References

Burjánek, J., Gassner-Stamm, G., Poggi, V., Moore, J. R., & Fäh, D., 2010. Ambient vibration analysis of an unstable mountain slope, *Geophysical Journal International*, **180**(2), 820–828.

Burjánek, J., Moore, J. R., Yugsi Molina, F. X., & Fäh, D., 2012. Instrumental evidence of normal mode rock slope vibration, *Geophysical Journal International*, **188**(2), 559–569.

Edwards, B., Michel, C., Poggi, V., & Fäh, D., 2013. Determination of Site Amplification from Regional Seismicity: Application to the Swiss National Seismic Networks, *Seismological Research Letters*, **84**(4), 611–621.

Fäh, D., Kind, F., & Giardini, D., 2001. A theoretical investigation of average H/V ratios, *Geophysical Journal International*, **145**(2), 535–549.

Fäh, D., Wathelet, M., Kristekova, M., Havenith, H.-B., Endrun, B., V., G. S., Poggi, Burjanek, J., & Cornou, C., 2009. Using ellipticity information for site characterisation using ellipticity information for site characterisation, *Technical report, NERIES JRA4*.

Hobiger, M., Bard, P.-Y., Cornou, C., & Le Bihan, N., 2009. Single station determination of Rayleigh wave ellipticity by using the random decrement technique (RayDec), *Geophysical Research Letters*, **36**(14), n/a–n/a, L14303.

Hobiger, M., Cornou, C., Wathelet, M., Giulio, G. D., Knapmeyer-Endrun, B., Renalier, F., Bard, P.-Y., Savvaidis, A., Hailemikael, S., Le, B. N., Ohrnberger, M., & Theodoulidis, N., 2013. Ground structure imaging by inversions of rayleigh wave ellipticity: sensitivity analysis and application to european strong-motion sites, *Geophysical Journal International*, **192**(1), 207–229.

Lontsi, A. M., Ohrnberger, M., Krüger, F., & Sánchez-Sesma, F. J., 2016. Combining surface wave phase velocity dispersion curves and full microtremor horizontal-to-vertical spectral ratio for subsurface sedimentary site characterization, *Interpretation*, **4**(4).

Park, C. B., Miller, R. D., & Xia, J., 1999. Multichannel analysis of surface waves, *Geophysics*, **64**(3), 800–808.

Poggi, V. & Fäh, D., 2010. Estimating rayleigh wave particle motion from three-component array analysis of ambient vibrations, *Geophysical Journal International*, **180**(1), 251–267.

Sambridge, M., 1999. Geophysical inversion with a neighbourhood algorithm—i. searching a parameter space, *Geophysical Journal International*, **138**(2), 479–494.

Scherbaum, F., Hinzen, K.-G., & Ohrnberger, M., 2003. Determination of shallow shear wave velocity profiles in the Cologne, Germany area using ambient vibrations, *Geophysical Journal International*, **152**(3), 597–612.

Socco, L. V. & Strobbia, C., 2004. Surface wave methods for near-surface characterisation: A tutorial, *Near Surface Geophysics*, **2**, 165–185.

Wathelet, M., 2008. An improved neighborhood algorithm: Parameter conditions and dynamic scaling, *Geophysical Research Letters*, **35**(9).